

## Direct evidence of antiferromagnetic exchange interaction in Fe(001) films: Strong magnon softening at the high-symmetry $\bar{M}$ point

Y. Meng,<sup>1</sup> Kh. Zakeri,<sup>1,\*</sup> A. Ernst,<sup>1,2</sup> T.-H. Chuang,<sup>1</sup> H. J. Qin,<sup>1</sup> Y.-J. Chen,<sup>1</sup> and J. Kirschner<sup>1,3</sup>

<sup>1</sup>Max-Planck-Institut für Mikrostrukturphysik, Weinberg 2, 06120 Halle, Germany

<sup>2</sup>Wilhelm Ostwald Institut für Physikalische und Theoretische Chemie, Universität Leipzig, Linnéstrasse 2, 04103 Leipzig, Germany

<sup>3</sup>Institut für Physik, Marthin-Luther-Universität Halle-Wittenberg, 06120 Halle, Germany

(Received 25 February 2014; revised manuscript received 12 November 2014; published 26 November 2014)

We report on the direct observation of a large unusual antiferromagnetic exchange interaction in Fe(001) films. By measuring the magnon dispersion relation over the entire Brillouin zone of an ultrathin Fe(001) film on Rh(001), we demonstrate that the signature of this unusual antiferromagnetic exchange interaction can be observed at the high-symmetry  $\bar{M}$  point. The exchange parameters are quantified by comparing the measured magnon dispersion relation with the results of our first-principles calculations. We suggest a way of examining the existence of an antiferromagnetic exchange interaction in layered magnetic structures and also a way of quantifying its strength.

DOI: [10.1103/PhysRevB.90.174437](https://doi.org/10.1103/PhysRevB.90.174437)

PACS number(s): 75.30.Ds, 75.50.Bb, 75.70.Ak, 75.70.Rf

### I. INTRODUCTION

Magnetism in low dimensions is a fascinating topic in condensed matter physics. In addition to the dimensionality aspects, i.e., the reduction of the symmetry of the system, the effects associated with the change of the chemical environment have an important impact on the properties of a low-dimensional magnet. As a result, numerous kinds of magnetic structures from simple ferromagnetic (FM) and antiferromagnetic (AFM) structures to very complex noncollinear spin structures have already been predicted and observed [1–4]. The formation of any kind of magnetic structure is the result of competing magnetic energies in the system, determining the magnetic ground state. It has been of great importance to find out which interactions compete in a given system, forming that specific magnetic ground state.

One of the most important magnetic interactions is the magnetic exchange interaction, which plays a governing role in the determination of the magnetic state of the system. In bulk ferromagnets, the exchange interaction is usually of FM character, whereas a very complex pattern of exchange parameters is expected in low-dimensional ferromagnets. This leads to the fact that the properties of low-dimensional magnets are inherently different than their bulk counterparts. Although much effort has been devoted to the observation and quantification of magnetic couplings in low-dimensional magnets, still, in the most common systems widely used in spintronics, namely, layered magnetic structures, the exchange interaction cannot be easily probed. A quantitative measure of the strength of the exchange interaction in magnetic thin films is necessary to understand and predict the behavior of layered magnetic structures. In particular, when the system exhibits an unusual pattern of exchange parameters, which can lead to very exotic magnetic states, this knowledge is of great importance.

In this paper we show that the signature of the unusual pattern of exchange coupling constants in ultrathin magnetic films can be observed by looking at the dynamics of the system, i.e., probing the magnetic excitations (magnons). As

an example we present the experimental results of an ultrathin Fe film grown on Rh(001). We show how the unusual exchange interaction can lead to a peculiar behavior of the magnon dispersion relation. We will further illustrate how the unusual pattern of exchange parameters can be quantified by comparing the experimental magnon dispersion relation to the results of first-principles calculations. In addition to that, we shed light on the longstanding question regarding the possibility of having an AFM exchange interaction in Fe films. We argue that although a film may show a *typical ferromagnetic hysteresis loop*, the pattern of exchange parameters can be extremely complicated. We also comment on the magnetic state of Fe films on Rh(001) in the ultrathin regime.

### II. EXPERIMENTS

All the experiments were performed in an ultrahigh vacuum chamber with a base pressure of  $3 \times 10^{-11}$  mbar. Prior to film deposition, the surface of the Rh(001) substrate was cleaned by cycles of Ar ion sputtering at 1.5 kV and a subsequent annealing at 900 K for 4 min [5]. Fe films with different thicknesses were grown by molecular beam epitaxy at 300 K. After the deposition of Fe, the samples underwent a slight annealing in order to improve the structural quality. The structural quality of both the Rh(001) surface as well as the Fe films was checked by means of low-energy electron diffraction (LEED). The sharp ( $1 \times 1$ ) LEED spots, observed for films with a thickness of up to 6 monolayers (ML), indicate a pseudomorphic growth of Fe on Rh(001), meaning that the in-plane lattice constant of the Fe films is exactly the same as the nearest neighbor distance of the Rh(001) surface atoms.

The magnetic properties of the films were investigated by means of the magneto-optical Kerr effect (MOKE). The angle of the incident and scattered laser beam with respect to the film normal was  $45^\circ$ . The measurements were performed in the longitudinal geometry at room temperature. The external magnetic field was applied along the Fe[1 $\bar{1}$ 0] direction.

The magnetic excitations were investigated by means of spin-polarized high-resolution electron energy loss spectroscopy (SPEELS) [6], a unique technique which has

\*zakeri@mpi-halle.de

successfully been applied to measure the high wave-vector magnons in ultrathin magnetic films [7–13]. All the SPEELS experiments were performed at room temperature. The sample was magnetized before the measurements and the spectra were recorded at the remanent state. In the SPEELS experiments, spin-polarized electrons with a given energy and momentum are scattered from a magnetic surface, and the energy and momentum of the scattered electrons are analyzed for the two possible spin orientations of the incident electrons (parallel and antiparallel to the sample magnetization). Usually, the intensity of the scattered electrons is recorded as a function of the energy loss in a given scattering geometry. Due to the conservation of the total angular momentum, the magnons can only be excited by incident electrons of minority spin character.

### III. RESULTS

The MOKE hysteresis loops recorded on Fe films of different thicknesses are presented in Fig. 1(a). For the films with a thickness of 4–6 ML, one observes a rectangular hysteresis loop. The hysteresis loop changes towards an S-shaped loop when the films are thicker than 6 ML. The Kerr ellipticity in remanence ( $M_r$ ) and saturation ( $M_s$ ) is plotted as a function of the film thickness in Fig. 1(b). The change in the slope of  $M_r$  at about 6 ML is due to the change in the film structure. Such a behavior has also been reported for Fe films on Ir(001) at a film thickness of 10 ML, where the structural transformation takes place [14].

In the SPEELS experiments, the scattering plane was chosen to be parallel to the Fe[100] and Fe[110] directions, which correspond to the  $\bar{\Gamma}$ - $\bar{X}$  and  $\bar{\Gamma}$ - $\bar{M}$  directions in the reciprocal space, respectively. The length of  $\bar{\Gamma}$ - $\bar{X}$  is  $1.17 \text{ \AA}^{-1}$ , and that of  $\bar{\Gamma}$ - $\bar{M}$  is  $1.65 \text{ \AA}^{-1}$ . Two examples of the SPEELS spectra recorded at an in-plane wave-vector transfer of  $\Delta K_{\parallel} = 1.05 \text{ \AA}^{-1}$  along the Fe[100] and Fe[110] directions are shown in Figs. 2(a) and 2(b), respectively.  $I_{\downarrow}$  ( $I_{\uparrow}$ ) represents the intensity of scattered electrons when the incoming beam polarization is parallel (antiparallel) to the sample magnetization. Due to the conservation of the total angular momentum during the scattering process, the magnons are only excited by incidence of minority electrons. This fact leads to a peak in the loss region of  $I_{\downarrow}$ . The magnon excitation peak can be clearly

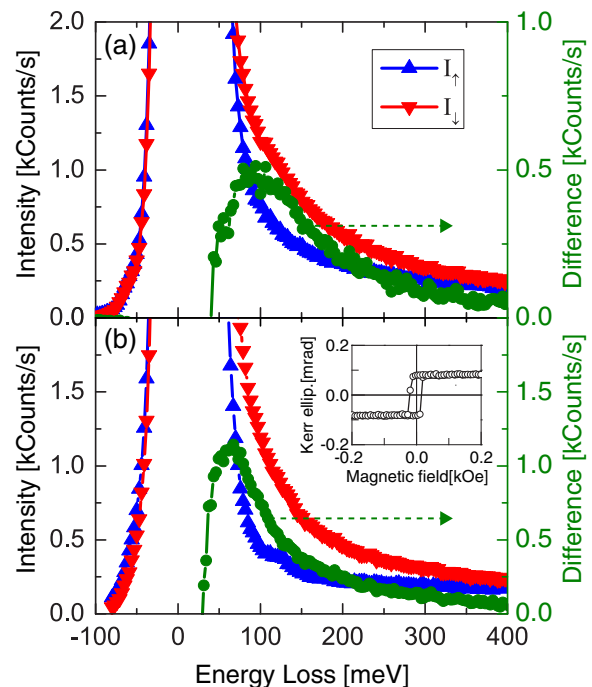


FIG. 2. (Color online) SPEELS spectra recorded at an in-plane wave-vector transfer of  $\Delta K_{\parallel} = 1.05 \text{ \AA}^{-1}$  probed along the (a) [100] and (b) [110] directions.  $I_{\downarrow}$  ( $I_{\uparrow}$ ) represents the intensity of the scattered beam when the spin polarization of the incident beam is parallel (antiparallel) to the magnetization. The difference spectra ( $I_{\text{Diff.}} = I_{\downarrow} - I_{\uparrow}$ ) are shown by solid circles. The magnetic hysteresis loop, measured with the field applied along the [110] direction, is shown in the inset.

seen in the difference spectrum ( $I_{\text{Diff.}} = I_{\downarrow} - I_{\uparrow}$ ). The peak at 85 meV in Fig. 2(a) and at 57 meV in Fig. 2(b) is associated with the magnon excitations.

A series of difference spectra recorded at various wave-vector transfers along both the  $\bar{\Gamma}$ - $\bar{X}$  and  $\bar{\Gamma}$ - $\bar{M}$  directions is shown in Fig. 3. The magnon peak shows a clear dispersion while changing the wave vector. Along the  $\bar{\Gamma}$ - $\bar{X}$  direction, the magnon peak moves towards higher energies as the wave vector increases up to the zone boundary (at  $1.17 \text{ \AA}^{-1}$ ). The peak position moves towards lower energies while further

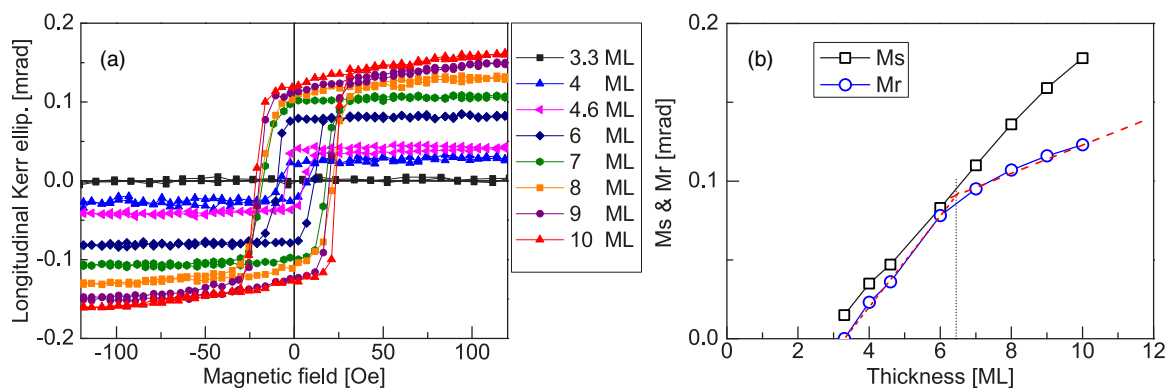


FIG. 1. (Color online) (a) The magnetic hysteresis loops recorded on Fe films of different thicknesses grown on Rh(001). The magnetic field was applied along the [110] direction. (b) Kerr ellipticity as a function of the Fe thickness in saturation ( $M_s$ ) and in remanence ( $M_r$ ). The change in the slope of  $M_r$  at about 6 ML is due to the structural relaxations.

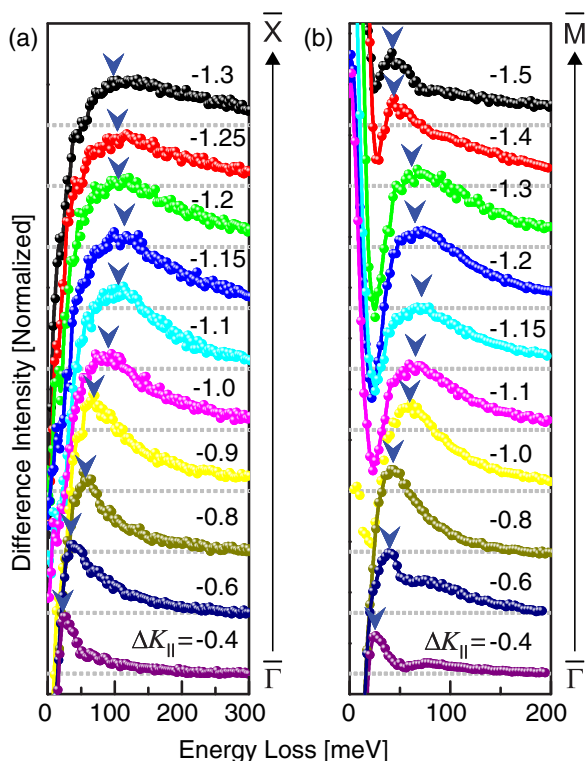


FIG. 3. (Color online) A series of difference spectra ( $I_{\text{Diff.}} = I_{\perp} - I_{\parallel}$ ) recorded at different wave-vector transfers  $\Delta K_{\parallel}$  along the (a)  $\bar{\Gamma}$ - $\bar{X}$  and (b)  $\bar{\Gamma}$ - $\bar{M}$  directions. The values of  $\Delta K_{\parallel}$  are given next to each spectrum in  $\text{\AA}^{-1}$ . The spectra are shifted upwards for a better comparison. The small arrows denote the magnon excitation energies.

increasing the wave vector. This is the indication of reaching the second Brillouin zone. As expected, due to the translational symmetry of the two-dimensional Brillouin zone, the magnon energy decreases beyond the first Brillouin zone. The key observation is the unusual behavior of the magnon energy versus the wave vector along the  $\bar{\Gamma}$ - $\bar{M}$  direction. Initially, the magnon peak moves to higher energies as the wave vector increases up to about  $1.15 \text{ \AA}^{-1}$ , and then it moves to lower energies when further increasing the wave vector. This is unexpected since  $1.15 \text{ \AA}^{-1}$  is not the zone boundary. Details of this unusual behavior will be discussed below.

The magnon dispersion relation is obtained by plotting the magnon energy versus the wave vector (open symbols in Fig. 4). The surface Brillouin zone is depicted in the inset. The magnon energies are rather low, even lower than the case of Fe/Ir(001) [15]. At small wave vectors, due to the large contribution of the quasielastic peak and also the finite experimental resolution, it is difficult to precisely extract the magnon energies for values lower than 25 meV. Along the  $\bar{\Gamma}$ - $\bar{X}$  direction, the magnon energy shows a monotonic dependence on the wave vector and reaches a maximum value of 102 meV at the  $\bar{X}$  point. The peculiar behavior is only observed along the  $\bar{\Gamma}$ - $\bar{M}$  direction. At  $\Delta K_{\parallel} = 0.4 \text{ \AA}^{-1}$ , the magnon energy is about 25 meV, which increases to a maximum value of 65 meV at  $\Delta K_{\parallel} = 1.15 \text{ \AA}^{-1}$ . It decreases to a value of 42 meV at the  $\bar{M}$  point. Obviously, such behavior is not expected for normal ferromagnets with positive (ferromagnetic) exchange parameters. The strong softening of magnons close to the

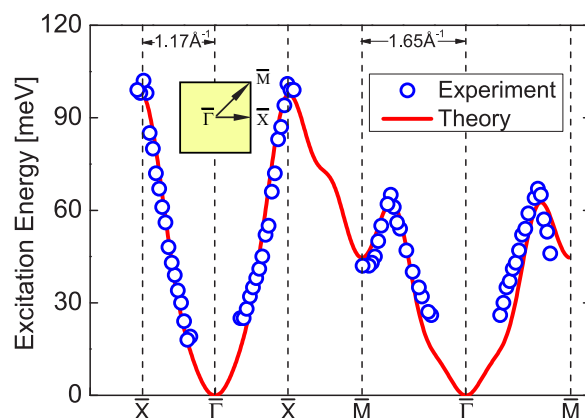


FIG. 4. (Color online) The experimental (open symbols) and theoretical (solid curve) magnon dispersion relation. Only the lowest-energy mode is shown. The surface Brillouin zone is depicted in the inset.

high-symmetry  $\bar{M}$  point is a signature of a complex pattern of magnetic exchange parameters in the system.

In order to understand the observed magnon softening at the  $\bar{M}$  point and also to quantify the exchange parameters, first-principles calculations were performed within the generalized gradient approximation of the density function theory [16]. The interatomic distances, used as the input of our calculations, were taken from the available experimental data.<sup>1</sup> We used a self-consistent Green's function method, especially designed for semi-infinite layered structures [17]. The interatomic exchange constants were calculated by employing the so-called magnetic force theorem, similarly implemented within a Green's function formalism [18]. The calculated dispersion relation of the acoustic mode (the mode with the lowest energy) is shown by the solid curve in Fig. 4. The results of the calculations are in very good agreement with the experimental results.

One can show that under some circumstances the lowest-energy magnon mode of an ultrathin film can be mainly localized at the interface. Let us consider a single element ferromagnetic film composed of  $n$  atomic layers. In such a case one would expect to observe  $n$  magnon modes, which can be associated with different parts of the film. If one assumes that the surface and interface are identical (this is the case for a free-standing film without a substrate), one would obtain two low-energy magnon modes which are degenerated at the high-symmetry points. However, the presence of the substrate leads to the fact that the surface and interface atomic layers are not equivalent and breaks the degeneracy of the two low-energy magnon modes. The lowest-energy mode will be mainly localized in the atomic layer with smaller exchange

<sup>1</sup>The values of the interlayer spacing are reported in Refs. [25,31]. In our calculations we used an Fe-Rh interlayer spacing of  $d_{\text{Fe-Rh}} = 1.70 \text{ \AA}$  and an Fe-Fe interlayer spacing of  $d_{\text{Fe-Fe}} = 1.66 \text{ \AA}$ . Our calculations for  $d_{\text{Fe-Rh}} = d_{\text{Fe-Fe}} = 1.66 \text{ \AA}$  revealed that a small variation of  $d_{\text{Fe-Rh}}$  has no effect on the strong magnon softening at the  $\bar{M}$  point. Only the absolute values of the magnon energies are slightly smaller for smaller  $d_{\text{Fe-Rh}}$ .

parameters. In the case of ferromagnetic films on nonmagnetic substrates, there are cases in which the exchange parameters in the interface atomic layer are smaller than the ones in the surface atomic layer. This is the case for the Fe/Rh(001) system and could be verified by calculating the Bloch spectral function of the different magnon modes of the system. It turned out that, although the contribution of the interface atomic layer to the lowest-energy mode is the highest, the other layers contribute to this mode as well. Since this mode has a finite spectral weight in the atomic layers on top (and also in the surface atomic layer), it can be excited with electrons. In addition, different magnon modes have different lifetimes. The adiabatic approaches do not provide any information regarding the lifetimes of different magnon modes. Calculations based on time-dependent density functional theory have shown that the lowest-energy magnon mode has the longest lifetime and shall appear as a sharp peak in the SPEELS spectra [15]. The higher-energy magnon modes are heavily damped because of their decay into the single-particle Stoner excitations and appear as broad features in the spectra. The contribution of all the other magnon modes to the difference spectra is greatly reduced due to their strong damping (short lifetime). The magnon mode in Fig. 4 is the lowest-energy mode, which is usually referred to as the acoustic mode. There are higher-energy magnon modes in the system which appear as a tail and shoulder after this lowest-energy magnon mode.

#### IV. DISCUSSION

The calculated values of the exchange coupling constants are presented in Fig. 5. For simplicity, we only show and discuss the exchange parameters up to the tenth nearest neighbors. In the surface layer (layer index VI), the first (+13), second (+2.5), fourth (+0.5), fifth (+0.6), sixth (+1), and tenth (+0.2) nearest neighbor intralayer exchange constants, describing the interaction between atoms in the same atomic plane, are positive, whereas the third (−2.5), seventh (−0.2), and ninth (−0.3) nearest neighbor intralayer exchange parameters are negative [Fig. 5(a)]. The eighth nearest neighbor intralayer exchange parameter is nearly zero (the absolute value is smaller than 0.1 meV). In the interface layer (layer index I), the first (−1.7), third (−0.8), fourth (−0.2), and sixth (−0.8) nearest neighbor intralayer exchange parameters are negative and only the second (+1.2) and seventh (+0.3) nearest neighbor ones are positive, meaning that an AFM exchange interaction is the dominating interaction in this layer [Fig. 5(b)]. The other intralayer exchange parameters in this layer are nearly zero. Our results indicate that the spin structure of 1 ML Fe/Rh(001) can be rather complicated, as reported recently [5]. The interlayer exchange parameters, describing the interaction between layers, show also a very complex pattern. The first (+17.4), second (+13), and fifth (+3) nearest neighbor interlayer exchange constants describing the coupling of layer I to the top layers are positive, whereas the third (−3.2), fourth (−2), sixth (−0.1), seventh (−0.5), eighth (−0.4), ninth (−0.2), and tenth (−1.1) nearest neighbor interlayer exchange constants (coupling this layer to the top layers) are negative. The interlayer exchange constants describing the coupling of layer VI to the layers below are mainly of FM character and only the third (−1.9), fourth (−2),

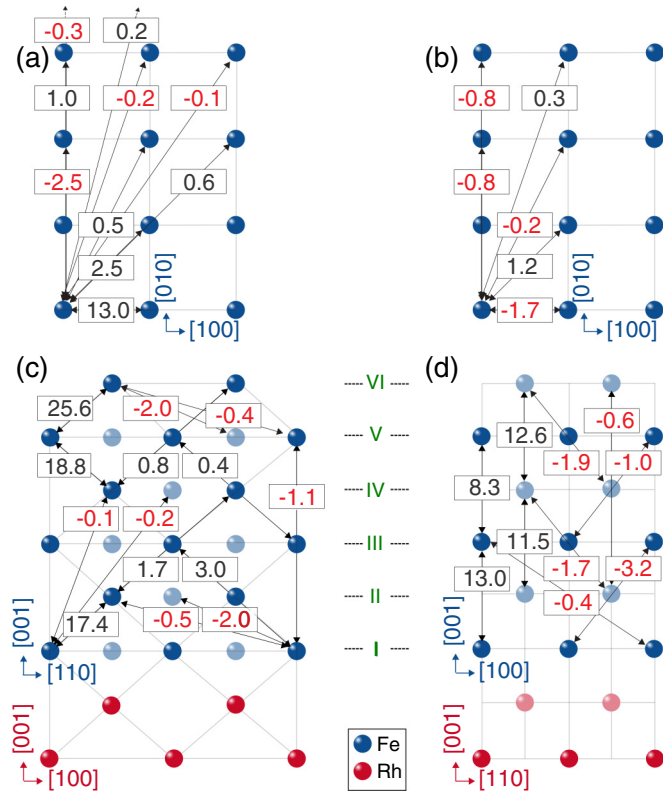


FIG. 5. (Color online) The calculated intralayer exchange parameters in (a) the surface layer VI and in (b) the interface layer I. A cut parallel to (c) the Fe(110) plane and (d) the Fe(100) plane with corresponding interlayer exchange parameters. The light color represents the atoms in the lower atomic plane. All the exchange parameters are given in meV.

seventh (−0.4), and tenth (−0.6) nearest neighbor interlayer exchange constants are negative [see Figs. 5(c) and 5(d)].

It is shown by calculations based on the many-body perturbation theory that a tetragonal distortion can lead to a strong magnon softening in tetragonally distorted bulk FeCo compounds [19]. Our first-principles calculations revealed that the complex pattern of exchange parameters (and also the peculiar behavior of the magnon dispersion relation) is a consequence of both tetragonal distortion and also interfacial electronic hybridizations at the Fe/Rh(001) interface. It is known that for the case of ultrathin films grown on a substrate, due to the interfacial electronic hybridizations, the properties of the interface layer are substantially different from the other layers [15,20–23]. Consequently, it is expected that the exchange coupling constants in the interface layer are significantly different than in the other layers. It is apparent from Figs. 5(a) and 5(b) that the exchange coupling constants at the interface are substantially smaller than the ones at the surface. As a result, the main contribution to the lowest-energy magnon mode is coming from the interface layer. The calculated atomic resolved spectral function revealed this fact. Such behavior has also been observed in the case of Fe/Ir(001) [15].

In order to shed light on the nature of the unusual pattern of exchange parameters in Fe films on Rh(001), we carefully investigated the layer-, orbital-, and spin-resolved density

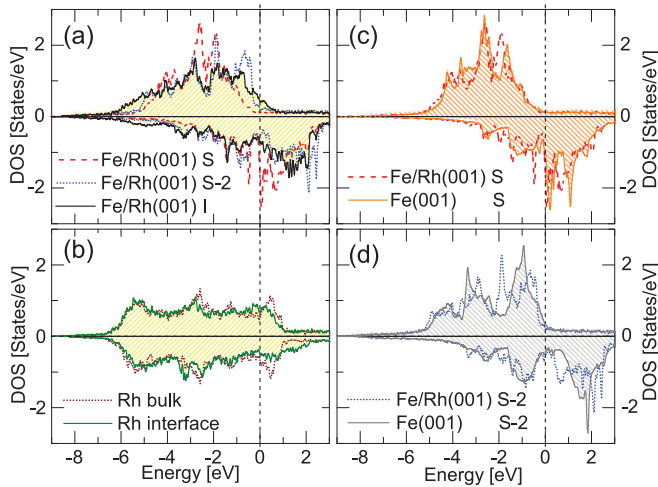


FIG. 6. (Color online) (a) Spin-resolved density of states of Fe atoms sitting in the surface layer, S (dashed curve), in the second layer below the surface, S-2 (dotted curve), and in the interface Fe layer, I (solid curve), of the Fe/Rh(001) system. (b) Spin-resolved density of states of Rh atoms sitting in the bulk Rh (dotted curve) and in the interface Rh layer (solid curve) in the Fe/Rh(001) system. (c) Spin-resolved density of states of Fe atoms sitting in the surface layer of the Fe film on Rh(001), S (dashed curve), and in the surface layer of Fe(001), S (solid curve). (d) Spin-resolved density of states of Fe atoms sitting in the second layer below the surface layer of the Fe film on Rh(001), S-2 (dotted curve), and in the second layer below the Fe(001) surface, S-2 (solid curve).

of states (DOS) of the system and compared them to the DOS of the semi-infinite Fe(001). In Fig. 6 we present and compare the DOS of atoms sitting in five different places of the Fe(001)/Rh(001) system: (i) in the topmost Fe layer (surface S), (ii) in the second Fe layer below the surface layer of the Fe film (S-2), (iii) in the interface Fe layer (I), (iv) in the interface Rh layer, and (v) in the bulk Rh. We compare the results to the ones of the Fe atoms sitting at the surface and in the second layer below the surface of the semi-infinite Fe(001) with a bulk lattice constant. As is apparent from Fig. 6(a), both spin-up and spin-down states of the interface Fe atoms are spread over a larger energy range, compared to the states of the Fe atoms sitting in the other Fe layers. In addition, a large number of spin-up states exist near the Fermi level. Such states are absent in the DOS of the Fe atoms sitting in the surface layer of the Fe film on Rh(001) and also in the DOS of the Fe atoms sitting in layer S-2 of the film [see Fig. 6(a)]. The orbital-resolved DOS revealed that these states are mainly of  $d_{yz}$  and  $d_{xz}$  character (or  $\Delta_5$  symmetry). The two sharp peaks in the spin-up states of the surface Fe atoms at energies of  $-1.9$  and  $-2.7$  eV are of  $d_{z^2}$  and  $d_{xz}$  ( $d_{yz}$ ) character, respectively. These states are suppressed and slightly shifted in the DOS of the interface Fe atoms. The spin-down density of states of the interface Fe atoms is also different from the ones of the Fe atoms sitting in the surface layer of the film. The sharp surface state, located just slightly above the Fermi level in the spin-down DOS of the Fe atoms sitting in the surface layer, is not present in the case of the Fe atoms sitting in the interface Fe layer. Also, the peak at about  $0.7$  eV, which is mainly of

$d_{z^2}$  character, is shifted to much higher energies ( $1.4$  eV) and is broadened in the case of Fe atoms in the interface Fe layer.

Comparing the density of states of the interface Rh atoms with the ones of the bulk Rh reveals that the spin-up states in the interface Rh atoms are at lower energies with respect to the same states in the atoms sitting in the Rh bulk. The spin-down states of the interface Rh atoms are at higher energies with respect to the states of the bulk Rh atoms [see Fig. 6(b)]. A large upward shift (about  $1.5$  eV) occurs for the spin-down states of  $d_{z^2}$  character. The sharp states at about  $-3.2$  eV in the interface Rh atoms are of  $d_{x^2-y^2}$  and  $d_{xz}$  ( $d_{yz}$ ) character. It is due to a downward shift of the same states located at about  $-2.6$  eV in the DOS of the bulk Rh atoms. The states at about  $-2.5$  eV in the spin-down states of the interface Rh atoms are mainly of  $d_{xy}$ ,  $d_{xz}$ , and  $d_{yz}$  character. These states are not so pronounced in the spin-down DOS of the bulk Rh atoms.

All the features mentioned above are an indication of the strong electronic hybridizations at the interface of Fe and Rh. The electronic hybridizations have a direct consequence on the magnetic exchange interaction of the system, especially on the interaction between Fe atoms located at the interface.

Comparing the DOS of Fe atoms located in the surface layer of the Fe films on Rh(001) to the DOS of Fe atoms located at the surface of Fe(001) with a bulk lattice constant shows substantial differences [see Fig. 6(c)]. For example, the sharp spin-up states at about  $-1.65$  eV in the DOS of the Fe atoms sitting in the surface layer of Fe(001) are of  $d_{z^2}$  character. These states are at about  $-1.9$  in the DOS of the Fe atoms in the surface layer of the Fe film on Rh(001). The spin-up states at about  $+1$  eV in the DOS of the Fe atoms at the Fe(001) surface are of the same character ( $d_{z^2}$ ). These states are shifted to  $+0.7$  eV in the DOS of the Fe atoms sitting at the surface of the Fe film grown on Rh(001). The minority surface state just above the Fermi level is also slightly shifted downwards when comparing the Fe(001) surface to the surface of the tetragonally distorted Fe(001) film on Rh(001). The differences in the spin-up states of the atoms sitting in the inner part of the film (layer S-2) compared to the states of the atoms sitting in layer S-2 of the semi-infinite Fe(001) are caused by an upward shift of  $d_{x^2-y^2}$ ,  $d_{xz}$ , and  $d_{yz}$  orbitals [see Fig. 6(d)]. The shift is about  $0.3$  eV for the  $d_{x^2-y^2}$  orbitals and about  $0.6$  eV for the  $d_{xz}$  and  $d_{yz}$  orbitals. Interestingly, a similar shift of the same orbitals causes the differences between the spin-down states of the Fe atoms in layer S-2 of the film and the spin-down states of the S-2 layer of semi-infinite Fe(001). All these shifts, which are the result of the tetragonal distortion, alter the interatomic exchange interaction, since the overlap of the electronic wave functions is modified via tetragonal distortion of the lattice.

In order to address the impact of the film structure on the magnon dispersion relation and, in particular, on the magnon softening observed at the  $\bar{M}$  point, we have performed calculations for different interlayer distances. The calculations are performed for the following cases and the results are summarized in Fig. 7(a):

$$\begin{aligned}
 \text{A: } & d_{\text{Fe-Rh}} = 1.44 \text{ \AA}, & d_{\text{Fe-Fe}} &= 1.44 \text{ \AA}. \\
 \text{B: } & d_{\text{Fe-Rh}} = 1.56 \text{ \AA}, & d_{\text{Fe-Fe}} &= 1.56 \text{ \AA}. \\
 \text{C: } & d_{\text{Fe-Rh}} = 1.60 \text{ \AA}, & d_{\text{Fe-Fe}} &= 1.60 \text{ \AA}. \\
 \text{D: } & d_{\text{Fe-Rh}} = 1.63 \text{ \AA}, & d_{\text{Fe-Fe}} &= 1.63 \text{ \AA}. \\
 \text{E: } & d_{\text{Fe-Rh}} = 1.71 \text{ \AA}, & d_{\text{Fe-Fe}} &= 1.56 \text{ \AA}.
 \end{aligned}$$

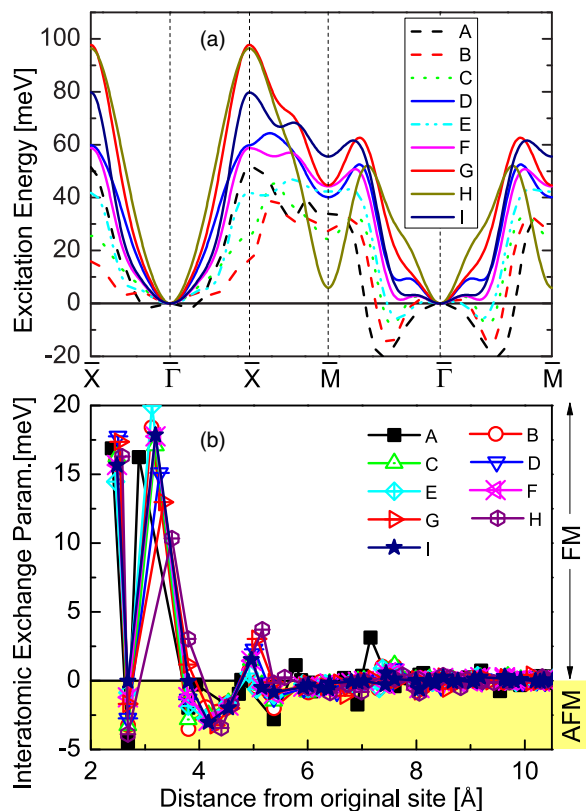


FIG. 7. (Color online) (a) The magnon dispersion relation calculated for 6 ML Fe on Rh(001) using different interlayer distances, as discussed in the text. For all cases a magnon softening at the  $\bar{M}$  point is observed. (b) The calculated  $\text{Fe}_I\text{-Fe}_{II}$  interatomic exchange parameters.  $\text{Fe}_I$  is sitting in the interface layer and  $\text{Fe}_{II}$  is sitting in the distance  $r$  from the  $\text{Fe}_I$  atom. The calculations are performed for different cases, as discussed in the text. The notation is the same as in (a). For all cases, a large AFM contribution to the exchange interaction is observed.

$$\begin{aligned}
 \text{F: } & d_{\text{Fe-Rh}} = 1.71 \text{ \AA}, & d_{\text{Fe-Fe}} = 1.60 \text{ \AA}. \\
 \text{G: } & d_{\text{Fe-Rh}} = 1.74 \text{ \AA}, & d_{\text{Fe-Fe}} = 1.66 \text{ \AA}. \\
 \text{H: } & d_{\text{Fe-Rh}} = 1.74 \text{ \AA}, & d_{\text{Fe-Fe}} = 1.74 \text{ \AA}. \\
 \text{I: } & d_{\text{Fe-Rh}} = 1.76 \text{ \AA}, & d_{\text{Fe-Fe}} = 1.60 \text{ \AA}.
 \end{aligned}$$

For all cases we find that a large contribution to the magnetic exchange interaction is of AFM character [see Fig. 7(b)]. This fact can be clearly concluded from the magnon softening at the  $\bar{M}$  point. Cases A, B, C, and E show negative magnon energies in the midway of the  $\bar{\Gamma}$ - $\bar{M}$  direction, and these cases are unrealistic. Although in cases D, F, H, and I the AFM exchange interaction manifests itself in the magnon softening at the  $\bar{M}$  point, the experimental magnon dispersion relation fits case G (and also the results of Fig. 4). Changing the value of the interlayer distance between the first Fe layer and Rh by  $\pm 0.04$  Å does not change the overall shape of the magnon dispersion relation—only the absolute values of the magnon energies

change by a few percent. The main feature, namely, the softening at the  $\bar{M}$  point, remains unchanged. The experimental magnon dispersion relation can be explained very well when the lattice constants  $d_{\text{Fe-Rh}} = 1.70$  Å,  $d_{\text{Fe-Fe}} = 1.66$  Å are taken into consideration (see Fig. 4). This fact indirectly indicates that the assumed structure parameters are correct. It should be pointed out that even without the first-principles calculations, and only based on the experimental results and using a simple Heisenberg model, one can conclude the existence of a large AFM exchange interaction in the system. If all the exchange parameters are positive, the energy of the high-symmetry  $\bar{M}$  point has to be larger than the other points of the Brillouin zone. The observed unusual magnon softening at the  $\bar{M}$  point can only be explained when the negative exchange parameters are considered. The advantage of the first-principles calculations is that they provide detailed information on the origin of the AFM exchange interaction.

Experimentally, different magnetic structures such as AFM [24], magnetic “dead layer” [25,26], and complex AFM have been suggested for Fe films [5] (and also FeCo/Rh multilayers [27,28]) on Rh(001). The magnetic exchange parameters have not been measured in any of those experiments. Theoretical calculations have predicted that the AFM configuration is favored for the Fe monolayer [29,30]. Our direct measurements of the exchange coupling parameters reveal, quantitatively, the importance of the large AFM exchange interaction in the system, which can lead to a complex AFM ground state for the Fe monolayer. The results clearly indicate that the pattern of exchange parameters can be very complicated, although the hysteresis loop is rectangular.

## V. CONCLUSION

In conclusion, we demonstrated that the unusual exchange coupling constants in layered structures have a direct consequence on the magnon dispersion relation. The softening of the magnons at high-symmetry points would reveal the existence of such an unusual exchange interaction in the system. Comparing the experimental results with the ones of first-principles calculations leads to a quantitative determination of such unusual exchange coupling constants. In addition to the fact that the results give a clear answer to the longstanding question regarding the possibility of having an AFM exchange interaction in Fe films, they suggest a way to probe and quantify the exchange parameters in ultrathin magnetic films and layered magnetic structures.

## ACKNOWLEDGMENTS

Funding from the Deutsche Forschungsgemeinschaft (DFG) is acknowledged by A.E. (priority program SPP 1538 “Spin Caloric Transport”). The calculations were performed at the Rechenzentrum Garching of the Max Planck Society. Fruitful discussions with Masaki Takada and Pedro Lana Gastelois are gratefully acknowledged.

[1] L. Sandratskii, *Adv. Phys.* **47**, 91 (1998).

[2] C. L. Gao, U. Schlickum, W. Wulfhekel, and J. Kirschner, *Phys. Rev. Lett.* **98**, 107203 (2007).

[3] K. von Bergmann, M. Bode, A. Kubetzka, O. Pietzsch, E. Vedmedenko, and R. Wiesendanger, *Philos. Mag.* **88**, 2627 (2008).

- [4] W. Wulfhekel and C. L. Gao, *J. Phys.: Condens. Matter* **22**, 084021 (2010).
- [5] M. Takada, P. Lana Gastelois, M. Przybylski, and J. Kirschner, *J. Magn. Magn. Mater.* **329**, 95 (2013).
- [6] H. Ibach, D. Bruchmann, R. Vollmer, M. Etzkorn, P. S. A. Kumar, and J. Kirschner, *Rev. Sci. Instrum.* **74**, 4089 (2003).
- [7] R. Vollmer, M. Etzkorn, P. S. A. Kumar, H. Ibach, and J. Kirschner, *Phys. Rev. Lett.* **91**, 147201 (2003).
- [8] W. X. Tang, Y. Zhang, I. Tudosa, J. Prokop, M. Etzkorn, and J. Kirschner, *Phys. Rev. Lett.* **99**, 087202 (2007).
- [9] K. Zakeri, Y. Zhang, J. Prokop, T.-H. Chuang, N. Sakr, W. X. Tang, and J. Kirschner, *Phys. Rev. Lett.* **104**, 137203 (2010).
- [10] Y. Zhang, P. Buczek, L. Sandratskii, W. X. Tang, J. Prokop, I. Tudosa, T. R. F. Peixoto, K. Zakeri, and J. Kirschner, *Phys. Rev. B* **81**, 094438 (2010).
- [11] K. Zakeri, Y. Zhang, T.-H. Chuang, and J. Kirschner, *Phys. Rev. Lett.* **108**, 197205 (2012).
- [12] Y. Zhang, T.-H. Chuang, K. Zakeri, and J. Kirschner, *Phys. Rev. Lett.* **109**, 087203 (2012).
- [13] K. Zakeri, *Phys. Rep.* **545**, 47 (2014).
- [14] T.-H. Chuang, K. Zakeri, A. Ernst, Y. Zhang, H. J. Qin, Y. Meng, Y.-J. Chen, and J. Kirschner, *Phys. Rev. B* **89**, 174404 (2014).
- [15] K. Zakeri, T.-H. Chuang, A. Ernst, L. Sandratskii, P. Buczek, H. Qin, Y. Zhang, and J. Kirschner, *Nat. Nanotechnol.* **8**, 853 (2013).
- [16] J. P. Perdew, K. Burke, and M. Ernzerhof, *Phys. Rev. Lett.* **77**, 3865 (1996).
- [17] M. Lüders, A. Ernst, W. M. Temmerman, Z. Szotek, and P. J. Durham, *J. Phys.: Condens. Matter* **13**, 8587 (2001).
- [18] A. Liechtenstein, M. Katsnelson, V. Antropov, and V. Gubanov, *J. Magn. Magn. Mater.* **67**, 65 (1987).
- [19] E. Şaşıoğlu, C. Friedrich, and S. Blügel, *Phys. Rev. B* **87**, 020410(R) (2013).
- [20] R. B. Muniz, A. T. Costa, and D. L. Mills, *J. Phys.: Condens. Matter* **15**, S495 (2003).
- [21] A. T. Costa, R. B. Muniz, and D. L. Mills, *Phys. Rev. B* **74**, 214403 (2006).
- [22] H. J. Qin, K. Zakeri, A. Ernst, T.-H. Chuang, Y.-J. Chen, Y. Meng, and J. Kirschner, *Phys. Rev. B* **88**, 020404 (2013).
- [23] L. Bergqvist, A. Taroni, A. Bergman, C. Etz, and O. Eriksson, *Phys. Rev. B* **87**, 144401 (2013).
- [24] C. Hwang, A. K. Swan, and S. C. Hong, *Phys. Rev. B* **60**, 14429 (1999).
- [25] K. Hayashi, M. Sawada, A. Harasawa, A. Kimura, and A. Kakizaki, *Phys. Rev. B* **64**, 054417 (2001).
- [26] K. Hayashi, M. Sawada, H. Yamagami, A. Kimura, and A. Kakizaki, *J. Phys. Soc. Jpn.* **73**, 2550 (2004).
- [27] F. Yildiz, M. Przybylski, and J. Kirschner, *Phys. Rev. Lett.* **103**, 147203 (2009).
- [28] M. Przybylski, J.-M. Tonnerre, F. Yildiz, H. C. N. Tolentino, and J. Kirschner, *J. Appl. Phys.* **111**, 07C103 (2012).
- [29] D. Spišák and J. Hafner, *Phys. Rev. B* **73**, 155428 (2006).
- [30] A. Al-Zubi, G. Bihlmayer, and S. Blügel, *Phys. Rev. B* **83**, 024407 (2011).
- [31] A. M. Begley, S. K. Kim, F. Jona, and P. M. Marcus, *Phys. Rev. B* **48**, 1786 (1993).